Biosynthesis of Silver and Iron Oxide Nanoparticles Using Moringa oleifera Seed Extractand Their Applications for Water Purification

Payam Bayazeed Hassan[a]*
payam.hassan@univsul.edu.iq
Honey Azad Saliha
Sanarya Amid Mohammeda
Larin Abdalqadir Ahmeda
Haider Mousa Hamzaha
Samir Mustafa Hamadb,
Rezan Omer Rasheeda
[a] Department of Biology, College of Science, University of Sulaimani, Sulaymaniyah, Kurdistan Region Iraq
[b] Scientific Research Centre, Soran University, Soran, Kurdistan Region, Iraq,
*Corresponding e-mail address:

Received Date:15-8-2025 Publication accepted date :21-9-2025

Abstract

Access to safe water for agricultural, industrial, and domestic applications remains a global challenge, with conventional methods often proving inadequate for emerging contaminants and antibiotic-resistant pathogens. This research presents a sustainable approach to water purification through the biosynthesis of silver nanoparticles (Ag NPs) and Iron oxide nanoparticles (Fe_3O_4 NPs) using *Moringa oleifera* seed extract. The biosynthesized nanoparticles were characterized using Fourier transform infrared (FTIR), powder X-ray diffraction (XRD), and Scanning Electron Microscopy (SEM) with Energy Dispersive X-Ray (EDX). Controlled synthetic water systems were used to test the nanoparticles' efficacy against *Escherichia coli* (ATCC 25922), *Pseudomonas aeruginos*a (ATCC 9027), a multidrug-resistant *Pseudomonas aeruginosa* isolate, and *Enterococcus faecalis*. The antibacterial activity of Ag NPs (500 µg/mL) was evaluated over various exposure durations (0, 30, 60, 120, and 180 minutes). Residual Ag NPs in treated synthetic water were removed using biosynthesized Fe_3O_4 NPs (5, 10, 15, and 20 mg/mL). The study shows that Ag NPs have a time-dependent, primarily bacteriostatic effect that progressively increases with exposure time against *E. coli* (ATCC 25922) and *E. faecalis* ,with inhibition of 59.58% and 94.70%, respectively, while also demonstrating a strong bactericidal effect against both *P. aeruginosa* strains from the earliest exposure, with inhibition reaching 100%. Furthermore, the synthesized Fe_3O_4 NPs demonstrated a high capacity to adsorb Ag NPs (94.01% removal efficiency). The results of this study support a dual-function strategy that utilizes nanoparticles synthesized via *Moringa oleifera* extract, where Ag NPs effectively eliminate pathogens and Fe_3O_4 NPs subsequently remove AgNP residues. This approach offers a promising, environmentally sustainable solution for comprehensive water purification.

Keywords: nanoparticles, water purification, bacteria, biosynthesis, environment

پوختە

دەستگەیشتن بە ئاوی سەلامەت بۆ بەکارهێنانی کشتوکاڵی، پیشەسازی و ناوخۆیی هێشتا تەحەدایەکی جیهانییە، لەگەڵ شێوازە ئاساییەکان زۆرجار دەیسەلمێنن کە ناتەواون بۆ پیسکەرەکانی سەرهەڵدان و مادە نەخۆشخوازەکانی بەرگریکار لە دژەزیندەییەکان. ئەم تۆیژینەوەیە ڕێگەیەکی بەردەوام بۆ پاککردنەوەی ئاو دەخاتە ڕوو لە ڕێگەی بایۆسێنتێزی نانۆگەردیلەکانی زیو (Ag NPs) و نانۆگەردیلەکانی ئۆکسیدی ئاسن (Fe3O4 NPs)بە بەکارهێنانی دەرهاویشتەی تۆوی مۆرینگا ئۆلیفێرا. نانۆگەردیلە بایۆسێنتێزکراوەکان بە بەکارهێنانی ژێر سووری گۆڕینی فۆریێ(FTIR) ، پەرشوبڵاوی تیشکی ئێکس پاودەر(XRD) ، و وردبینی ئەلکترۆنی سکانکردن (SEM)بە تیشکی ئێکس پەرشوبڵاوی وزە (EDX) تایبەتمەند کران. سیستەمی ئاوی دەستکردی کۆنترۆڵکراو بەکارهێنرا بۆ تاقیکردنەوەی کاریگەری نانۆگەردیلەکان دژی ئێشێریچیا کۆلای(ATCC 25922) ، سۆدۆمۆناس ئایرۆجینۆسا(ATCC 9027) ، جیاکراوەی سۆدۆمۆناس ئایرۆجینۆسا کە بەرگری لە فرە دەرمان دەکات، و ئینتێرۆکۆکۆسی پیکالیس. چالاکیی دژە بەکتریاکانی Ag NPs (500 میکرۆگرام/میلی لیتر) لە ماوەی بەرکەوتنی جیاوازدا (٠، ٣٠، ٦٠، ١٢٠، و ١٨٠ خولەک) هەڵسەنگێندرا. پاشماوەی Ag NPs لە ئاوی دەستکردی چارەسەرکراودا بە بەکارهێنانی Fe3O4 NPs بایۆسێنتێزکراو (٥، ١٠، ١٥، و ٢٠ میلیگرام/میلی لیتر) لابراون. تۆیژینەوەکە دەریدەخات کە Ag NPs کاریگەرییەکی وابەستە بە کات و بە شێوەیەکی سەرەکی بەکتریا وەستاندنی هەیە کە بەرەوپێشچوون زیاد دەکات لەگەڵ بەرکەوتنی کات دژی ئی.کۆلای (ATCC 25922) و ئی.فیکالیس، لەگەڵ ڕێگریکردن لە ٥٩.٥٨% و ٩٤.٧٠%، بە ڕێکەوت، لە هەمان کاتدا کاریگەرییەکی بەهێزی بەکتریاکوژی لە دژی هەردوو جۆری P. aeruginosa لە سەرەتاییترین نیشان دەدات بەرکەوتن، لەگەڵ ڕێگریکردن کە دەگاتە ١٠٠%. سەرەڕای ئەوە، Fe3O4 NPsدروستکراوەکان توانایەکی بەرزیان نیشان دا بۆ مژینی Ag NPs (94.01% کارایی لابردنی). ئەنجامەکانی ئەم تۆیژینەوەیە پشتگیری لە ستراتیژی دوو کارایی دەکەن کە نانۆگەردیلەکان بەکاردەهێنێت کە لە ڕێگەی دەرهاویشتەی مۆرینگا ئۆلیفێرا دروستکراون، کە Ag NPs بە شێوەیەکی کاریگەر مادە نەخۆشخوازەکان لەناو دەبات و Fe3O4 NPs دواتر پاشماوەی AgNP لا دەبات. ئەم ڕێبازە چارەسەرێکی بەڵێندەر و بەردەوام لە ڕووی ژینگەییەوە بۆ پاککردنەوەی ئاو بە شێوەیەکی گشتگیر پێشکەش دەکات.

وشەی سەرەکی: نانۆگەردیلە، پاککردنەوەی ئاو، بەکتریا، بایۆسێنتێز، ژینگە

ملخص

لا يزال الحصول على مياه مأمونة للاستخدامات الزراعية والصناعية والمنزلية يُمثل تحديًا عالميًا، حيث غالبًا ما تُثبت الطرق التقليدية عدم كفايتها في مواجهة الملوثات الناشئة ومسببات الأمراض المقاومة للمضادات الحيوية. يُقدم هذا البحث نهجًا مستدامًا لتنقية المياه من خلال التخليق الحيوي لجسيمات نانوية من الفضة (Ag NPs)وجسيمات نانوية من أكسيد الحديد (Fe3O4 NPs)باستخدام مستخلص بذور المورينجا أوليفيرا. وُصفت

الجسيمات النانوية المُخلّقة حيويًا باستخدام تقنية تحويل فورييه بالأشعة تحت الحمراء(FTIR) ، وحيود الأشعة السينية للمسحوق(XRD) ، والمجهر الإلكتروني الماسح (SEM) مع الأشعة السينية المشتتة للطاقة .(EDX) استُخدمت أنظمة مياه صناعية مُتحكم بها لاختبار فعالية الجسيمات النانوية ضد الإشريكية القولونية (ATCC 25922)، والزائفة الزنجارية(ATCC 9027) ، وهي عزلة من الزائفة الزنجارية المقاومة للأدوية المتعددة، والمكورات المعوية البرازية. قُيِّم النشاط المضاد للبكتيريا لجسيمات النانو الفضية (٥٠٠ ميكروغرام/مل) على مدى فترات تعرض مختلفة (٠، ٣٠، ٦٠، ١٢٠، و١٨٠ دقيقة)، أُزيلت جسيمات النانو الفضية المتبقية في المياه الصناعية المُعالجة باستخدام جسيمات النانو Fe3O4المُصنّعة بيولوجيًا (٥، ١٠، ١٥، و٢٠ ملغ/مل). أظهرت الدراسة أن جسيمات النانو الفضية (Ag NPs)لها تأثير مضاد للبكتيريا يعتمد على الزمن، ويزداد تدريجيًا مع مرور الوقت ضد الإشريكية القولونية (ATCC 25922) والإشريكية البرازية(E. faecalis) ، مع تثبيط بنسبة ٥٩.٥٨% و٩٤.٧٠% على التوالي، مع وصول التثبيط إلى ١٠٠%. علاوة على ذلك، أظهرت جسيمات النانو الفضية (Fe3O4)المُصنّعة قدرة عالية على امتصاص جسيمات النانو الفضية (كفاءة إزالة ٩٤.٠١%). تدعم نتائج هذه الدراسة استراتيجية ثنائية الوظيفة تستخدم جسيمات نانوية مُصنّعة من مستخلص المورينجا أوليفيرا، حيث تقضي جسيمات النانو الفضية بفعالية على مسببات الأمراض، بينما تُزيل جسيمات النانو الفضية (Fe3O4) بقايا جسيمات النانو الفضية. يقدم هذا النهج حلاً واعدًا ومستدامًا بيئيًا لتنقية المياه بشكل شامل.

الكلمات المفتاحية: جسيمات نانوية، تنقية المياه، بكتيريا، تخليق حيوي، بيئة

1. Introduction

Water is a valuable resource for humankind and the most important element for all life on Earth (Qu et al., 2013). Industrial pollutants, including heavy metals, toxic chemicals, and dyes, continue to contaminate soil and water systems, and this can be poisonous and

threaten the ecosystems (Qurbani and Hamzah 2021; Kyzas & Mitropoulos, 2021; Yass et al. 2024). Therefore, a robust system must be developed to ensure zero waste and environmental sustainability (Poornima et al., 2022). Chlorination is a popular and efficient method for disinfecting water. When chlorine reacts with natural materials in water, it creates toxic disinfection byproducts (DBPs). Trihalomethanes and haloacetic acids are two examples of DBPs that have been connected to risks for cancer, reproduction, and developmental health. Although chlorination keeps waterborne illnesses at bay, its drawbacks underscore the need for safer substitutes or methods to lower the production of DBP (Li & Mitch, 2017). In addition, due to the high cost and, in certain situations, inadequate treatment of wastewater by traditional wastewater treatment processes, novel strategies are continually being researched to enhance and augment conventional water treatment techniques (Sharma & Sharma, 2012). Nanotechnology holds considerable promise for advancing wastewater and water treatment by increasing the use of smaller molecules, which has major ecological consequences (Esakkimuthu, 2014).

As the field continues to advance, nanotechnology has emerged as a promising method for dye degradation and water purification, with catalyst nanoparticles serving as an essential component due to their increased surface area, reactivity, and distinctive size-dependent characteristics

(Qurbani et al. 2024). Their small size and high surface-to-volume ratio of nanoparticles give them extremely high absorption, interaction, and reaction properties (Prachi et al., 2013). Additionally, silver nanoparticles (AgNPs) are widely recognized for their unique optical, electronic, and antibacterial properties, enabling their use in biosciences to be more effectively and efficient (Vance et al., 2015). Such characteristics make Ag NPs common components in sanitizing, personal care, and textile compositions because they are utilized extensively as antimicrobials and antiseptics (Blaser et al., 2008; Chernousova and Epple, 2013; Lopez-Garcia et al., 2014). Such a biological process can be taken up as an alternative method for the synthesis of Ag NPs without leading to any environmental problem. Moreover, biologic synthesis has inherent advantages such as scaling, cost-effectiveness, and biocompatibility, making it an appropriate option for sustainable nanoparticle synthesis (Ahmed et al., 2018; Hamzah et al., 2018; Fattah et al., 2022; Mohammed and Hamzah, 2024). Plant extracts that have been employed for the biosynthesis of the Ag NPs are a more eco-friendly process (Haris & Ahmad, 2024). Different parts of plants (roots, stems, leaves, flowers, and seeds) of many plants, which are called medicinal plants, can be applied for the green synthesis of various kinds of metallic nanoparticles, including Ag NPs (Al Mashud et al., 2022).

Besides other phytochemicals that are involved in mediating metal ion bio-reduction during NPs synthesis and stabilization, they contain proteins, amino acids, lipids, and phenolics. The composition of biomolecules in the plant extract determines the NPs' size, shape, and morphology (Jiang et al., 2025). There are 13 species of moringa, which are known by a variety of common names depending on where they are grown (Mohammed & Hawar, 2022). The most commonly grown species of Moringa, the sole genus in the Moringaceae family, is *M. oleifera* (Brahmachari, 2001). The plant, which is indigenous to the southern foothills of the Himalayas in northwest India, grows quickly and can withstand drought (Dan-kishiya et al., 2023). It has several applications in the food, cosmetics, and pharmaceutical industries, as well as in bioremediation (water purification), and is well-known for its high nutritional value (Coelho et al., 2023). Alkaloids and proteins, which are very beneficial biomolecules that can serve as capping agents, were only found in the seeds, despite the fact that both the leaf and the seed had flavonoids and phenolics, according to the phytochemical analysis .*M. oleifera* seed (MOS) has garnered a lot of interest lately due to its benefits to rural economies and its superiority as a source of oil and other products. For approximately 40 years, MOS has garnered scientific attention for its conventional use in flocculating contaminants in water. Despite its great potential as a coagulant for water treatment, MOS lacks antimicrobial properties. Water treated with MOS is therefore unfit for human consumption without additional treatment (Mehwish et al., 2021).

Since heavy metals exist in both aquatic and soil environments, are non-biodegradable, and tend to build up in organisms, they become one of the major concerns, as they could be highly toxic and carcinogenic even in small quantities (Sun et al., 2018). However, according to studies done by Kiwumulo et al. (2022), Fe3O4 NPs are biodegradable and harmless to organisms. The large surface area, high number of active surface sites, low intraparticle diffusion rate, and high adsorption capacities of Fe3O4 NPs (nano-adsorbent particles) compared to conventional adsorbents make them a highly effective approach for treating contaminated water with heavy metals and dyes. Moreover, a permanent magnet can quickly remove them from the solution because of their high saturation magnetization levels (Gómez-Pastora et al., 2014).

This study aimed to employ *M. oleifera* seed extract for the green biosynthesis and characterization of silver nanoparticles (Ag NPs) and Iron oxide nanoparticles (Fe_3O_4 NPs), to

evaluate the antimicrobial efficacy of Ag NPs in wastewater treatment, and to utilize biosynthesized Fe_3O_4 NPs for the precipitation and removal of silver from treated water.

2. Materials & Methods

2.1. Preparation of *M. oleifera* Seed Extract

The seeds of *M. oleifera* were procured from the cultivation field of Dr. Jamal Saeed Rashid (Sulaymaniyah, Kurdistan Region), where the species is grown under controlled agricultural practices. 30 g of powdered *M. oleifera* seeds was taken and mixed with 300 mL of sterile distilled water. The solution was stirred using a magnetic stirrer on a hot plate. Following thermal extraction, the solution was allowed to cool and subsequently filtered through Whatman No. 1 filter paper to obtain a clear aqueous extract, which was used immediately for nanoparticle synthesis.

2.2. Biosynthesis of Silver (Ag NPs) and Iron (Fe_3O_4 NPs) Nanoparticles from *M. oleifera* Seed Extract

Silver nanoparticles were synthesized by adding 300 mL of the moringa seed extract to 600 mL of 1 mM silver nitrate ($AgNO_3$) solution. The mixture was placed under direct sunlight at room temperature for 24 hours to assist the reduction of Ag^+ ions from $AgNO_3$ and formation of MOS-Ag NPs (Varthini et al., 2018). Initially, the formation of Ag NPs was confirmed by a visible color change of the solution from light yellow to brown (Coelho et al., 2023). In addition to Ag NPs, the production of iron (III) nanoparticles was performed according to (Kiwumulo et al. 2022). 9.73 g of ferrous iron (III) oxide was mixed with 350 ml of distilled water. Subsequently, 350 mL of the *M. oleifera* seed extract was added to the mixture, the pH of the mixture was adjusted to 9, then incubated in a water bath for 1 hour at 60 °C to enhance the release and the activation of photochemicals. Following the incubation, the solution color changed from reddish brown to dark brown. Further, the confirmation of Ag NP and Fe_3O_4NP formation was recorded by UV–vis spectroscopy at (200-800) nm. Both solutions containing the synthesized nanoparticles were dried at 40°C for 72 hrs in a hot air oven. The resulting Ag NPs and Fe3O4 NPs powder were collected and stored in sterile containers.

2.3. Characterization Techniques

The most crucial and straightforward method to verify the bioreduction of nanoparticles is by UV-Vis spectroscopy. The colloidal sample's absorbance spectrum was measured between 200 and 800 nm using a UV–Vis spectrophotometer (Agilent Technologies Cary 60, USA). The biomolecules that were responsible for metal reduction and nanoparticle stability were identified using FTIR analysis. The silver nanoparticles' functional group was further examined using a Thermo Scientific Nicolet iS10 FTIR spectrometer in the 4000–400 cm^{-1} wavelength range. In addition, an X-ray diffractometer (PAN Analytical Xpert Pro, Netherlands) employing Cu-Kα radiation (λ = 1.54 Å) operating at 45 kV and 40 mA was used to examine the crystal structure of biosynthesized nanoparticles. All samples' diffracted intensities were measured using a step size of 0.1° and a scanning speed of 1 steps per second, throughout the 2θ range of 10º to 80º. Moreover, scanning electron microscopy (SEM) was used to examine the shape and dispersion of powdered nanoparticles (Quanta 4500, FEI). Energy Dispersive X-ray Spectroscopy (EDX) was used to verify the elemental silver and the cleanliness of the produced nanoparticles (Anandalakshmi, Venugobal, & Ramasamy, 2016; Ashrafi-Saiedlou, Rasouli-Sadaghiani, Fattahi, & others, 2025).

2.4. Antibacterial Activity of Biosynthesized Ag NPs

Four bacterial strains were employed to assess the antibacterial efficacy of the MOS-Ag NPs , including *E. coli* ATCC (25922), and *P. aeruginosa* ATCC (9027) as a quality control strain and clinical isolate of multidrug-resistant bacteria *P. aeruginosa*, *E. faecalis*. The antibacterial activity of MOS-Ag NPs was assessed using a synthetic water sample, as shown in Figure 1, following the methodology used by Moustafa (2017) with modifications. The synthetic ponds were subsequently inoculated with multidrug-resistant bacteria *P. aeruginosa*, *E. faecalis*, and standard strains *E. coli* ATCC (25922), and *P. aeruginosa* ATCC (9027). MOS-Ag NPs were re-dispersed in sterile distilled water, followed by sonication to obtain a homogeneous suspension. Each assay comprised 50 mL sterile distilled water (SDW) with 1 mL MOS-Ag NPs suspension and 150 µL standardized bacterial inoculum. Controls included positive (SDW + bacterial inoculum) and negative (SDW + MOS-Ag NPs). Aliquots (100 µL) were collected at 30, 60, 120, and 180 min, plated on nutrient agar, and incubated at 37°C. After a 24-hour incubation period, colony-forming units (CFUs) were enumerated to determine bacterial viability**.**

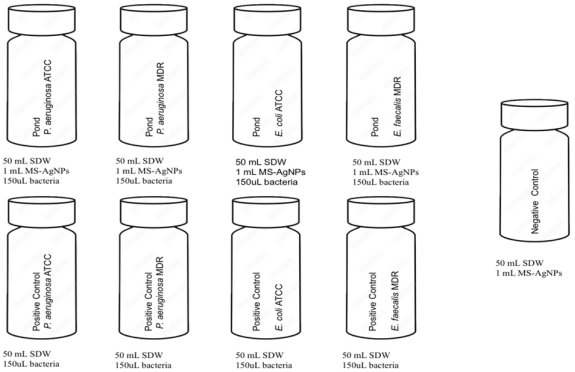

Figure 1. Experimental setup for antibacterial testing of MOS-Ag NPs. Each synthetic water sample, standardized bacterial inoculum, and MOS-AgNP suspension. Positive and negative controls were included**.**

2.5. Water Treatment Using Fe_3O_4 NPs

Residual silver nanoparticle and microbial debris removal was assessed by treating 5 mL aliquots from each bacterial pond with Iron oxide nanoparticles (5, 10, 15, or 20 mg), using the water treatment setup (Figure 2). Samples were vortexed, and at 30, 60, and 120 min, 200 µL was transferred to a 96-well plate. Additionally, 200 µL of the corresponding supernatant (post-centrifugation) was added to adjacent wells, and negative controls were included for comparison. An absorbance reading was done at 400 nm using a UV–Vis microplate reader to evaluate turbidity and removal efficiency**.**

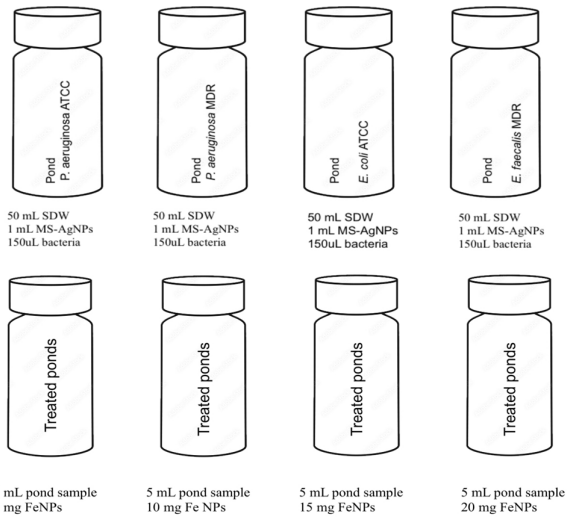

Figure 2. Water treatment setup using MOS-Fe_3O_4 NPs for the removal of residual Ag NPs and microbial debris. Treated samples were incubated with varying FeNP concentrations, vortexed, and analyzed for turbidity and removal efficiency**.**

2.6. Data Analysis for Removal Efficiency

For each treated synthetic water, 200 µL aliquots were transferred to a 96-well plate for absorbance measurement at 400 nm. Adjacent wells contained 200 µL of the corresponding supernatant obtained after centrifugation at designated time points (30, 60, and 120 minutes). This setup allowed comparison between total and precipitated particulates.

$$\%\, RE \;=\; \frac{(\,C_o - C_e\,)}{C_o} \;\times\; 100$$

Where RE is the removal efficiency, C_o is the initial absorbance of the treated sample, and C_e is the absorbance of the centrifuged supernatant. This reflects the proportion of bacteria and nanoparticles removed by Fe_3O_4 NPs, with higher values indicating greater removal performance.

3. Results

3.1. Biosynthesis of MOS-Ag NPs and MOS-Fe_3O_4 NPs

Silver nanoparticle formation was initially observed through a color change of the *M. oleifera* seed extract–silver nitrate mixture from light yellow to bronze brown after 24 hrs of exposure to sunlight, indicating Ag^+ reduction and nanoparticle nucleation (Figure 3). As for the biosynthesis of MOS-Fe_3O_4 NPs, upon mixing iron (III) oxide with the seed extract, the solution initially appeared reddish brown. Following incubation, the color deepened to a dark brown, indicating Fe^{3+} reduction and nanoparticle formation. After centrifugation and drying in the oven, the nanoparticles yielded a dark reddish-brown crystalline powder. The resulting nanoparticles exhibited magnetic properties, confirming the successful synthesis of magnetically responsive MOS-Fe_3O_4 NPs (Figure 4).

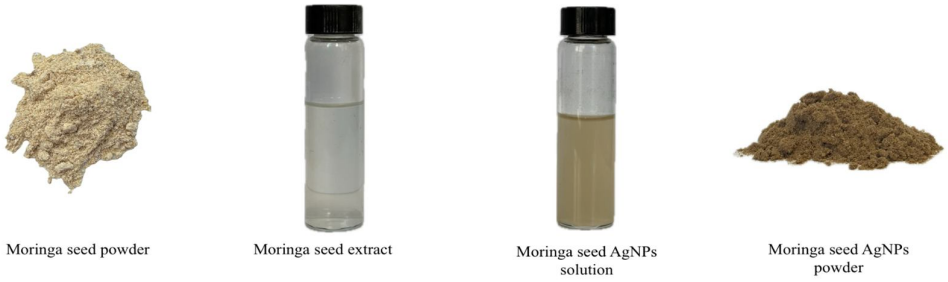

Figure 3. Visual confirmation of biosynthesized silver nanoparticles (MOS-Ag NPs). Light yellow to bronze-brown color change indicates Ag^{+} reduction and AgNP formation. Final dried powders exhibit metallic properties.

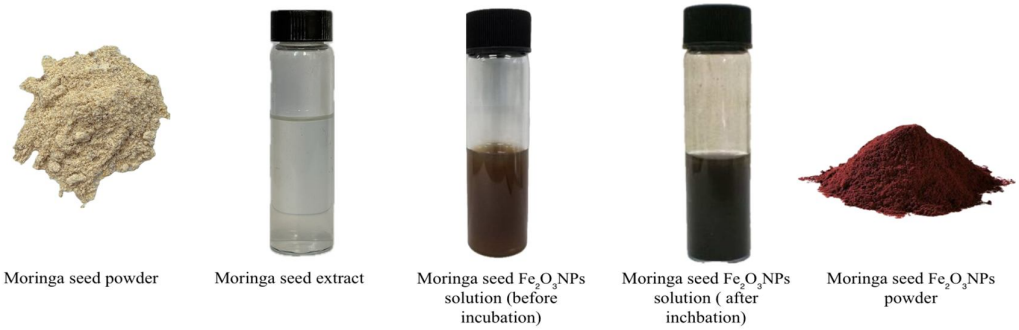

Figure 4. Visual confirmation of biosynthesized Iron oxide nanoparticles (MOS-Fe_3O_4 NPs). Reddish-brown to dark-brown color change indicates Fe^{3+} reduction and Fe_3O_4NP formation. Final dried powders exhibit magnetic properties.

3.2. Characterization of Biosynthesized Nanoparticles

Ag NP formation was further confirmed by UV-Vis spectroscopy, as shown in (Figure 5A), which showed a sharp absorbance peak at about 400 nm, followed by a slow decrease toward longer wavelengths. The peak indicates that the metallic silver nanoparticles' surface plasmon resonance (SPR) was successfully formed (Ahmed et al., 2016; El-Desouky et al., 2021). The main peak's high optical density (~4 OD) indicates a significant concentration of nanoparticles(Li et al., 2020). Furthermore, the Fe_3O_4NP spectra (Figure 5B) showed a broad absorbance band that gradually decreased in the range from ~230 to 300 nm, with a slight maximum in the middle. Iron oxide nanoparticles, which show UV absorption as a result of charge transfer transitions between Fe^{2+} and Fe^{3+} ions, are compatible with this profile (Bhattacharjee et al., 2023; Gowsalya et al., 2024). The non-plasmonic character of iron-based nanoparticles is consistent with the lack of noticeable visible-region peaks (Yew et al., 2023).

FTIR analysis was used to determine which bioactive compounds were in charge for reducing the silver ions in the *M. oleifera*-formed nanoparticles (Figure 5C). A prominent absorption band that is seen at 3300–3400 cm^{-1} is indicative of the O–H stretching vibrations of alcohols and phenols. The C-H stretching is indicated by the peak close to 2920 cm^{-1}. Proteins connected to the surface of the nanoparticle are shown by distinct bands at about 1650 cm^{-1} and 1540 cm^{-1}, which correspond to amide I (C=O stretching) and amide II (N–H bending/C–N stretching). Symmetric COO^{-} stretching is responsible for a characteristic around ~1440 cm^{-1}, whereas C–O or C–O–C

stretching vibrations from polysaccharides or other carbohydrate moieties are responsible for signals around ~1100–1130 cm^{-1} (Łach et al., 2023;). A band near ~1630–1650 cm^{-1} and a broad O–H stretching at ~3200–3400 cm^{-1} are indicative of adsorbed water or hydroxyl groups, according to the FTIR analysis of Fe_3O_4 NPs (Figure 5D). Peaks at ~1340 cm^{-1} and ~1110 cm^{-1}, which relate to biomolecule capping, correspond to organic functional groups like C–N, COO^- , and C–O/C–O–C. The presence of Iron oxide nanoparticles is confirmed by a noticeable absorption at about 560 cm^{-1}, which is indicative of Fe–O stretching vibrations (Łach et al., 2023; Lesiak et al., 2019; Bordbar, Moghdami, & Ghorbani, 2014).

The XRD analysis of Ag NPs can help analyze the exact nature of the nanoparticle; the graph in (Figure 5E) shows weak diffraction peaks at approximately 38°, 44°, and 65°, matching the (111), (200), and (220) crystallographic planes of face-centered cubic (fcc) silver (JCPDS card No. 04-0783). The low intensity and broadness of the peaks indicate a tiny nanoparticle size and/or the presence of amorphous organic capping (Chávez-Granados et al., 2024; Hua et al., 2024). Regarding the nature of Fe_3O_4 NPs, the XRD analysis according to (Figure 5F) displayed distinct diffraction peaks at ~34°, 38°, 44.5°, 53.5°, 57°, and 62° corresponding to the (220), (311), (400), (422), (511), and (440) planes of spinel iron oxide (either Fe_3O_4 or γ-Fe_2O_3). These sharp planes indicate the formation of crystalline Iron oxide nanoparticles, consistent with previous studies (Chen et al., 2017; Mohammadi et al., 2021).

The SEM images of Ag nanoparticles reveal polydisperse, quasi-spherical particles forming dense, porous agglomerates. Primary grains are in the nanometer range, while secondary aggregates range from submicron to several microns. The morphology is relatively uniform across the imaged regions. Additionally, the SEM micrographs of Fe_3O_4 NPs display rough, raspberry-like secondary particles formed from tightly packed nanosized grains. Clusters vary from ~1 μm to several μm in diameter, with occasional cracking observed in larger agglomerates. The EDX spectra analysis results (Figure 7A) for Ag reveal a dominant signal at 2.98 keV. Quantitative data for the tested region show 100% normalized mass and atomic percentages of Ag. The presence of the silver element but no silver ions indicates the complete reduction of Ag+ to Ag0, moreover the formation of Ag NPs using *M. Oleifera* seed extract. Depending on the EDX results, the produced Ag NPs are highly pure and crystalline (Aouf et al., 2024). The EDX spectrum (Figure 7B) of Iron oxide nanoparticles shows a significant signal for Fe at ~6.40 keV and O at ~0.525 keV. Quantitative analysis gives Fe at ~69.94 wt% (40 at%) and O at ~30.06 wt% (60 at%), closely matching the theoretical Fe_3O_4 stoichiometry. The considerable amounts of iron ions in the Iron oxide nanoparticles contribute to the successful formation of Fe_3O_4 NPs from *M. oleifera* seed extract (Jalal & Fakhre, 2021).

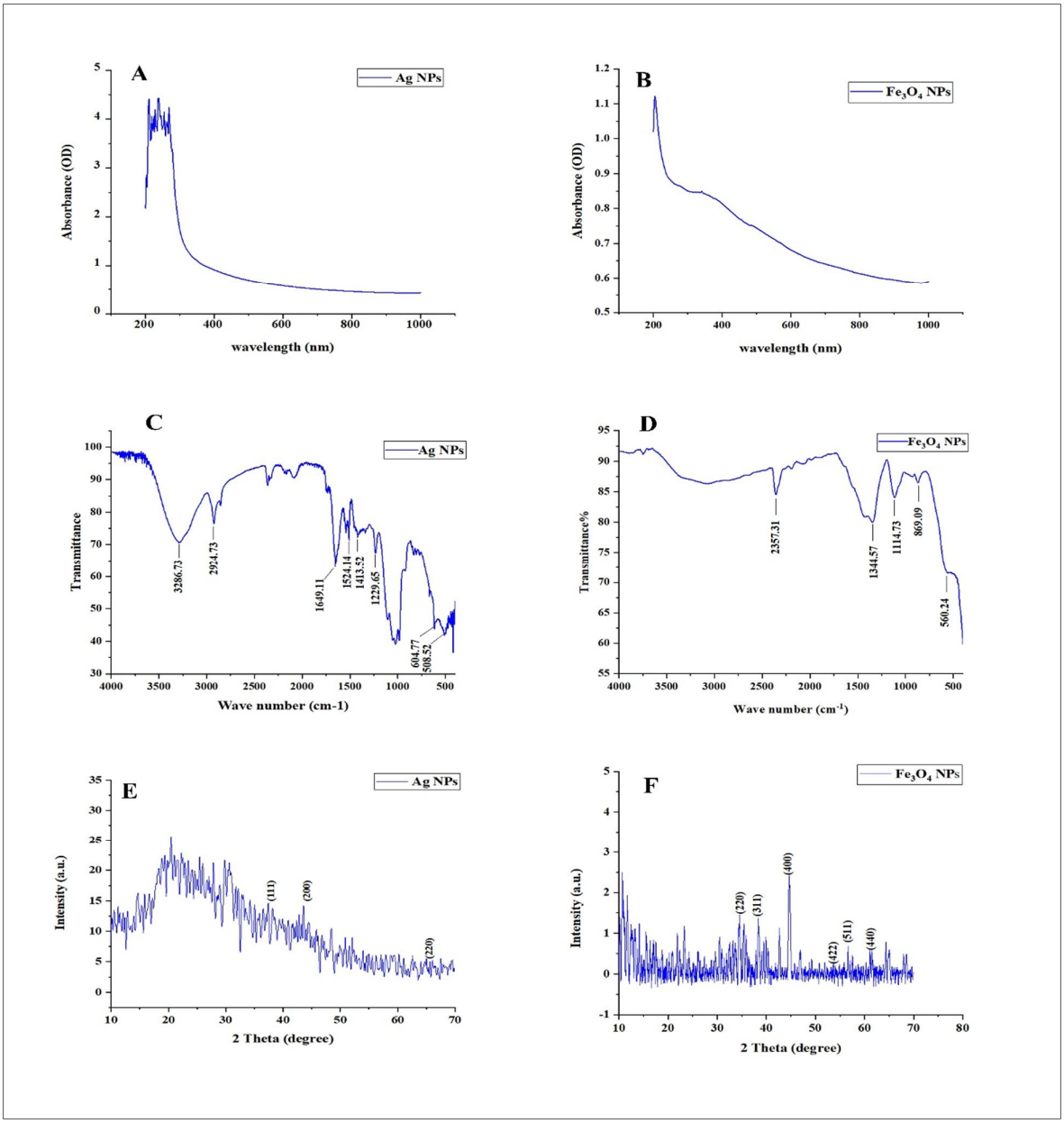

Figure 5. Characterization of biosynthesized nanoparticles. (**A**) UV–Vis spectrum of MOS-Ag NPs showing a surface plasmon resonance peak at ~400 nm. (**B**) UV–Vis spectrum of MOS-Fe_3O_4 NPs with broad absorbance at 230–300 nm. (**C**) FTIR spectrum of MOS-Ag NPs highlighting phenols, proteins (amide I/II), and polysaccharides. (**D**) FTIR spectrum of MOS-Fe_3O_4 NPs showing Fe–O vibrations and organic capping groups. (**E**) XRD pattern of MOS-Ag NPs with (111), (200), and (220) reflections of fcc silver. (**F**) XRD pattern of MOS-Fe_3O_4 NPs matching spinel iron oxide (Fe□O□/γ-Fe□O□) crystalline phases.

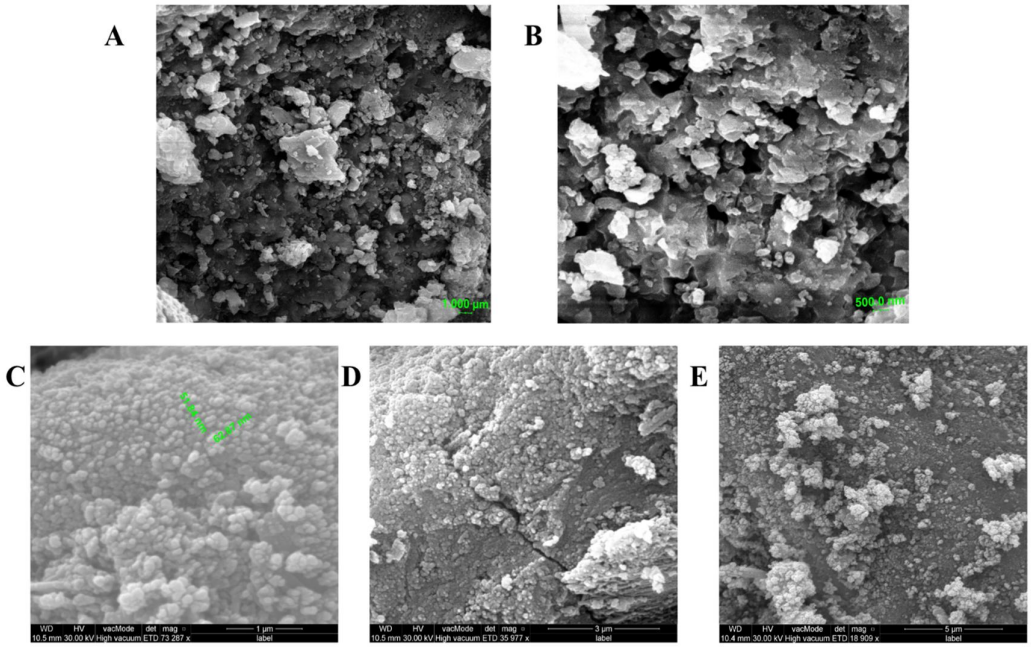

Figure 6. SEM images of MOS-Ag NPs (A, B) and MOS-Fe_3O_4 NPs (C–E) illustrating nanoscale morphology, size distribution, and particle aggregation.

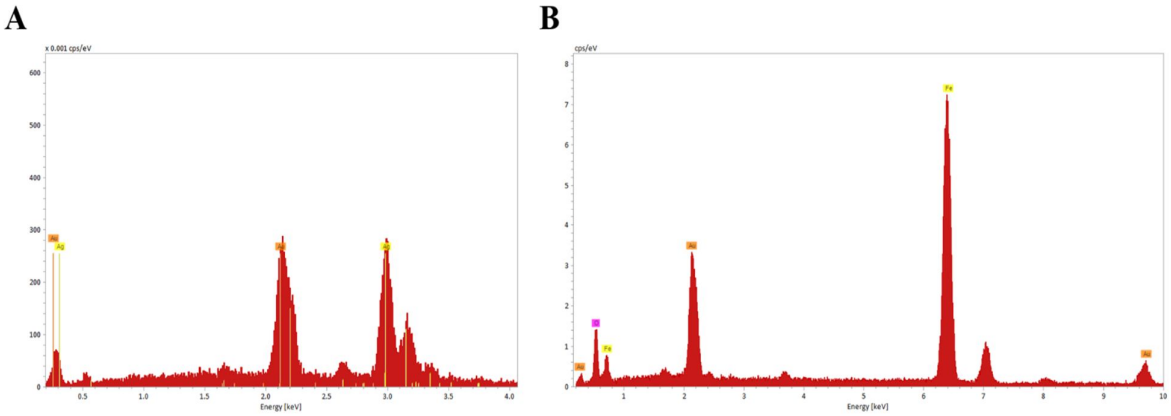

Figure 7. (**A**) EDX spectrum of silver nanoparticles, displaying prominent Ag Lα and Lβ peaks, confirming the presence of elemental silver with no detectable impurities. (**B**) EDX spectrum of Iron oxide nanoparticles,

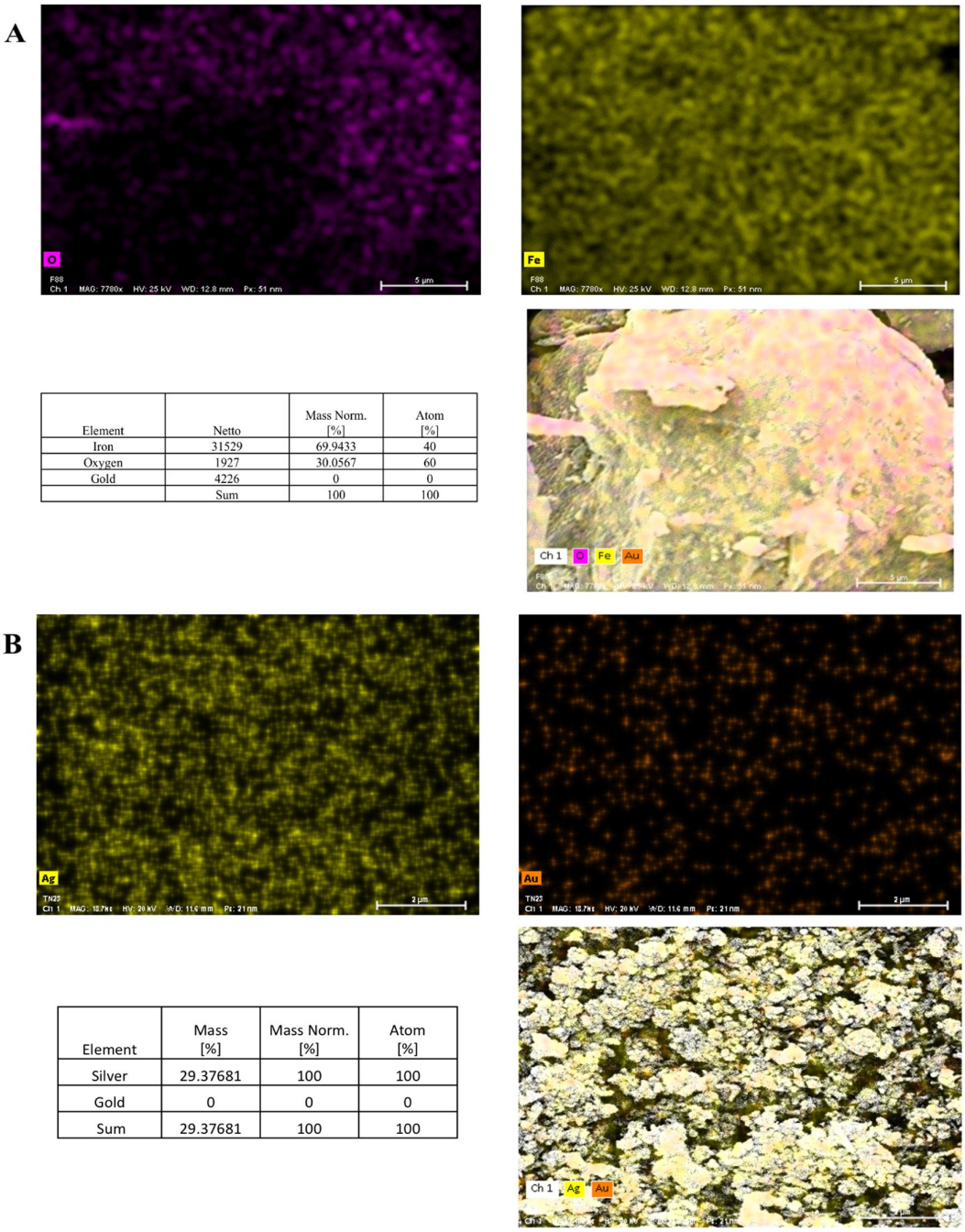

Element	Netto	Mass Norm. [%]	Atom [%]
Iron	31529	69.9433	40
Oxygen	1927	30.0567	60
Gold	4226	0	0
	Sum	100	100

Element	Mass [%]	Mass Norm. [%]	Atom [%]
Silver	29.37681	100	100
Gold	0	0	0
Sum	29.37681	100	100

Figure 8. (**A**) SEM micrographs, quantitative EDX data, and elemental mapping of silver nanoparticles. (**B**) SEM micrographs, quantitative EDX data, and elemental mapping of Fe nanoparticles

3.3. Antibacterial Activity of Biosynthesized Ag NPs

The antibacterial activity of *Moringa oleifera* mediated silver nanoparticles (MOS-Ag NPs) at 500 µg/mL was evaluated against multidrug-resistant bacteria *P. aeruginosa, E. faecalis,* and standard strains *E. coli* ATCC (25922)*, and P. aeruginosa* ATCC (9027)*,* over exposure times of 0, 30, 60, 120, and 180 minutes (Figure 9). Both *P. aeruginosa* ATCC (9027) and MDR strains

exhibited complete susceptibility from the initial contact, maintaining an inhibition ratio of 100% throughout the experimental period, indicating a rapid and sustained bactericidal effect.In contrast, *E. coli* ATCC (25922) showed a progressive inhibition, with the initial inhibition rate of 36.18% at 0 minutes, increasing to 59.68% after 180 minutes. Similarly, *E. faecalis* demonstrated high initial susceptibility (81.73%), gradually increasing to 94.70% at 180 minutes (Figure 9). These findings suggest that Ag NPs exert an immediate bactericidal effect against *P. aeruginosa* strains, while displaying a time-dependent, predominantly bacteriostatic activity against *E. coli* ATCC (25922) and *E. faecalis* .

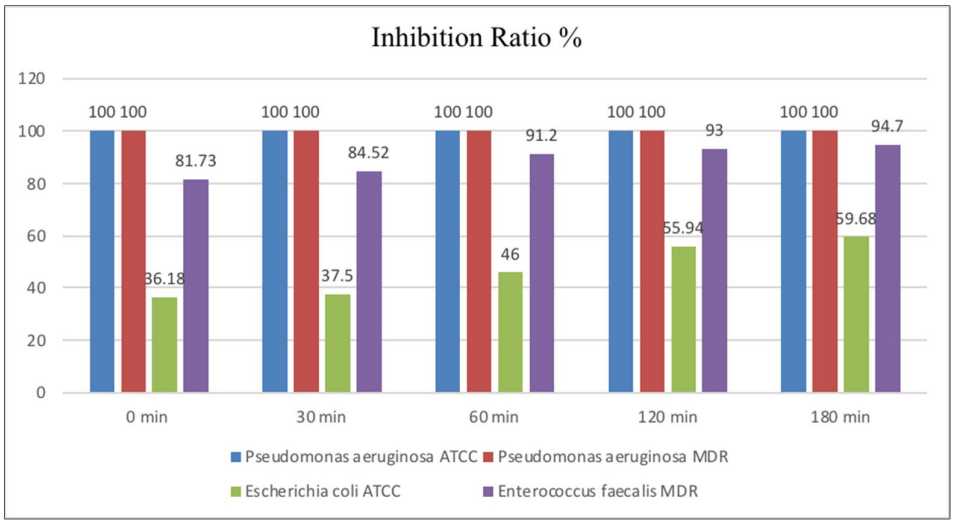

Figure 9. Antibacterial activity of MOS-Ag NPs (500 µg/mL) against *P. aeruginosa* ATCC (9027), P. aeruginosa , *E. coli* ATCC (25922), and *E. faecalis* over 0–180 min. *P. aeruginosa* strains showed complete inhibition from initial exposure, while *E. coli* and *E. faecalis* exhibited progressive, time-dependent inhibition**.**

3.4. Removal of Residual Ag NPs Using Biosynthesized Fe_3O_4 NPs

The adsorption capacity of *M. oleifera*-mediated Iron oxide nanoparticles (Fe_3O_4 NPs) for the removal of residual Ag NPs from treated synthetic water was evaluated at 5, 10, 15, and 20 mg/mL after 30 minutes of contact time (Figure 10). Removal efficiencies for *P. aeruginosa* ATCC (9027) ranged from 86.04% at 5 mg/mL to 91.12% at 20 mg/mL, while the MDR *P. aeruginosa* isolate showed slightly higher efficiencies (87.36–92.27%). For *E. coli* ATCC (25922), adsorption efficiencies increased from 89.08% at the lowest dosage to 94.16% at 20 mg/mL. *E. faecalis* exhibited slightly lower initial removal (84.26% at 5 mg/mL) but reached 94.01% at 20 mg/mL. Across all bacterial systems, Fe_3O_4 NPs demonstrated an apparent dosage-dependent increase in adsorption capacity, achieving more than 94% removal at 20 mg/mL (Figure 10). Overall, the results confirm the dual-function potential of *M. oleifera* nanoparticles in water purification. Ag NPs achieved complete and immediate elimination of *P. aeruginosa* strains and significant time-dependent inhibition of *E. coli* ATCC (25922) and *E. faecalis* . Subsequent treatment with Fe_3O_4 NPs effectively removed residual Ag NPs from the treated water, ensuring high antibacterial efficacy while minimizing nanoparticle residues, thus supporting a sustainable and comprehensive water treatment approach.

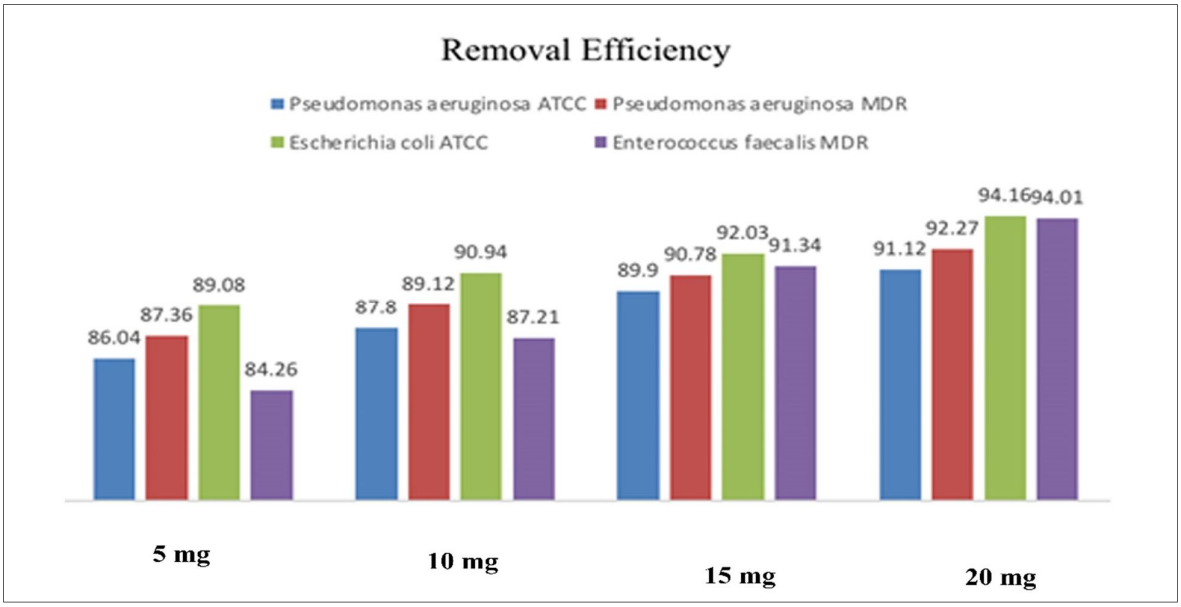

Figure 10. Removal efficiency of MOS-Fe_3O_4 NPs (5–20 mg/mL) for residual Ag NPs in synthetic water after 30 min. Data for *P. aeruginosa* ATCC 9027, *P. aeruginosa* MDR, *E. coli* ATCC 25922, *and E. faecalis* MDR indicate dose-dependent removal, with >94% efficiency at the highest concentration.

4. Discussion

In the present study, biosynthesis of silver and Iron oxide nanoparticles was carried out using *Moringa oleifera* seed extract. The visual color changes from light yellow to bronze brown for Ag NPs and reddish brown to dark brown for Fe_3O_4 NPs due to surface plasmon resonance phenomena which are associated with nanoparticle formation, confirming the reduction of Ag^+ and Fe^{3+} ions by phytochemicals present in the seed extract. The hydrophilic hydroxyl groups found in the phytochemicals attached to the surface of these nanoparticles enable the NPs to scatter and distribute uniformly in aqueous solutions (Kiwumulo et al., 2022). Similar visual cues have been widely reported in green synthesis studies (Coelho et al., 2023; Haris & Ahmad, 2024), underscoring the reliability of *M. oleifera* seeds as a reducing and capping agent source.

The optical response of Ag NPs is in line with reported SPR bands of 350–450 nm for spherical silver particles (Ahmed et al., 2016). Variations in peak position and width reflect differences in particle size, shape, and degree of aggregation (Li et al.). The sharp and intense SPR peak here suggests small spherical particles and a relatively narrow particle size distribution. In contrast, Fe3O4 NPs showed broad UV absorption without the presence of any sharp visible features, as is typical for Iron oxide nanoparticles. (Bhattacharjee et al., 2023; Gowsalya et al., 2024). These spectra are from ligand-to-metal charge transfer and d–d transitions rather than plasmonic resonance. The slope observed beyond 400 nm supports the presence of polydisperse iron oxide particles in varying oxidation states (Yew et al., 2023). The UV–Vis data strongly support the successful biosynthesis of Ag NPs and Fe_3O_4 NPs, with Ag NPs exhibiting clear plasmonic characteristics and Fe_3O_4 NPs displaying broad electronic transitions typical of iron oxides (Li et al., 2020; Ahmed et al., 2016; El-Desouky et al., 2021).

The FTIR and XRD data collectively confirm the successful synthesis of biogenic silver and Iron oxide nanoparticles; the presence of biomolecules stabilizes the nanoparticles derived from the plant

extract. In the analysis of the Ag NPs, the FTIR spectrum demonstrates the presence of surface-adsorbed biomacromolecules, including proteins (amide I/II), polysaccharides (C–O/C–O–C), and phenolic compounds (O–H, C=O), consistent with their role as reducing and stabilizing agents in green synthesis methods (Łach et al., 2023; Pasieczna-Patkowska et al., 2025). The XRD analysis confirms fcc metallic silver, referring to successful reduction of Ag^{+} to Ag^{0} nanoparticles (Chávez-Granados et al., 2024; Hua et al., 2024), with peak broadening consistent with nanoscale dimensions and organic capping.

For the Iron oxide nanoparticles, the FTIR profile with Fe–O stretching at ~560 cm^{-1} and signatures of organic capping correspond to the formation of iron-oxide cores coated by biomolecules (Łach et al., 2023; Lesiak et al., 2019; Bordbar et al., 2014). XRD characterization confirms a spinel structure observed for magnetite, suggesting a successful formation of crystalline Fe_3O_4 /γ-Fe_2O_3 nanoparticles (Chen et al., 2017; Mohammadi et al., 2021). Together, these results confirm the efficacy of the green synthesis method in producing well-defined, biomolecule-stabilized nanoparticles. The successful synthesis of silver nanoparticles (Ag NPs) using Moringa oleifera seed extract was validated by SEM analysis. In line with other studies on green synthesis, the micrographs showed primarily spherical to quasi-spherical particles with a small amount of aggregation (Ahmed et al., 2016; Khalil et al., 2014). This morphology is explained by the presence of phytochemical compounds, specifically proteins, polysaccharides, and phenolics, which served as capping and reducing agents, stabilizing the nanoparticles and regulating nucleation (Gurunathan et al., 2014). The measured particle size fell within the nanometer range, aligning with prior studies on *M. oleifera*-mediated AgNP synthesis (Mishra et al., 2020). Minor agglomeration frequently occurs in plant-mediated synthesis owing to elevated surface energy and potential incomplete capping (Rajeshkumar & Bharath, 2017).

The strong Ag peaks at ~3 keV confirm the purity of silver (Kortright & Thompson, 2001; Vernieres et al., 2021). The Au peaks are attributed to gold sputter coating for charge mitigation during SEM imaging (Thermo Fisher Scientific, 2019; Jeol USA, 2022) and are not indicative of contamination. The Fe:O ratio of ~40:60 at% matches closely with theoretical Fe_3O_4 stoichiometry (42.9:57.1), allowing for standard EDS uncertainties in oxygen quantification Karmakar et al., 2023). Co-located Fe and O signals confirm single-phase magnetite. Minor Au peaks are again linked to sputter coating . A notable difference was observed in microbial susceptibility profiles when evaluating antibacterial activity tests of biosynthesized MOS-Ag NPs . Both *P. aeruginosa* ATCC 9027 and *P. aeruginosa* MDR exhibited complete inhibition from initial exposure, suggesting a potent bactericidal mechanism, potentially involving the generation of reactive oxygen species and causing oxidative stress that damages cellular components and disrupts bacterial cell structure, and damages the cell wall, leading to leakage of intracellular contents, additionally interfering with DNA replication (Liao et al., 2019). Whereas *E. coli* ATCC (25922) and multidrug-resistant *E. faecalis* exhibited a time-dependent inhibition, showing a bacteriostatic effect that intensifies over extended contact. This variation could be attributed to structural differences between Gram-negative and Gram-positive bacterial envelopes, as well as strain-specific defence mechanisms (Chernousova & Epple, 2013; Dakal et al., 2016). The rapid bactericidal action against *P. aeruginosa* in particular highlights the potential of MOS-Ag NPs for controlling waterborne pathogens, including antibiotic-resistant strains. This variability likely stems from differences in cell wall architecture and defence systems among bacteria (Jiang et al., 2025,

Haris & Ahmad, 2024). Similar observations were made by (Moustafa, 2013). It was reported that silver nanoparticles from Penciillium Citreonigum Dierck and Scopulariopsis brumptii Salvanet, with a concentration of 676.9 mg/L, and contact times of 15 and 120 min, can remove all types of bacteria in polluted water.

In this study, the removal efficacy of biosynthesized Fe_3O_4 NPs effectively removes residual Ag NPs following antimicrobial treatment of synthetic water, thereby addressing a significant environmental challenge associated with nanoparticle-based disinfection, the contamination of treated water with nanoparticle residues (Ramirez et al., 2025). The adsorption efficiency of biosynthesized Fe_3O4 NPs in removing residual Ag NPs aligns with reported removal mechanisms such as electrostatic attraction and surface complexation typical of iron-based nanoparticles, as well as pH and Ag NPs concentration (Aragaw et al., 2021; Ramirez et al., 2025). Fe_3O4 NPs had adsorption capacities with over 94% removal efficiencies at a dose of 20 mg/mL, and showed improved adsorption performance in a dose-dependent manner. This removal process is assumed to be caused by electrostatic attraction between the positively charged surfaces of Fe_3O4 NPs and negatively charged Ag NPs, as well as van der Waals forces and the surface complexation phenomenon (Gutierrez et al., 2017; Maestri et al., 2017). The biosynthesis using M. oleifera seeds does not utilize toxic reagents and harsh conditions but is a low-cost and eco-friendly process, which can be carried out under mild conditions (Moodley et al., 2018; Haris & Ahmad, 2024). Therefore, the synergy of these two biosynthesized nanomaterials in a sequential treatment process, which marries intense antimicrobial activity with effective nanoparticle residue adsorption, is an innovative achievement in green nanotechnology for water purification systems (Kumar et al., 2024). It is important to note that factors like dissolved substances, suspended particles, and chemical interactions can influence nanoparticle behavior and efficacy. Further studies are needed to assess the long-term environmental fate, transformations, and ecotoxicity of Ag NPs and Fe_3O_4 NPs, as well as the regeneration, reuse, and scalability of FeNP adsorbents through field studies (Maestri et al., 2017; Madadi & Mokhtarani, 2024).

Conclusion

In conclusion, the current investigation showed that Ag NPs made with *M. oleifera* enable rapid and effective disinfection against pathogenic and multidrug-resistant bacteria, while the following application of the Fe_3O_4 NPs suggested efficient removal of residual nanoparticles. This green dual-functioning approach offers a promising and sustainable method for full and safe water treatment. However, our study does have some limitations. The experiments did not replicate the full complexities of natural waters, which could be impacted by factors such as organic matter, turbidity, or competing ions on the behavior, stability, and performance of nanoparticles. Therefore, additional research is required to determine the long-term environmental behavior, possible transformations, and ecotoxicological impacts of Ag NPs and Fe_3O_4 NPs in real-world applications. Future studies should seek to scale up the process, determine the regeneration and reuse potential of Fe NP adsorbents, and confirm performance through pilot and field studies, to aid the implementation of practical experiments.

References

- Ahmed, A. A., Hamzah, H., & Maaroof, M. (2018). Analyzing formation of silver nanoparticles from the filamentous fungus Fusarium oxysporum and their antimicrobial activity. Turkish Journal of Biology, 42(1), 54-62.
- Ahmed, S., Ahmad, M., Swami, B. L., & Ikram, S. (2016). A review on plants extract mediated synthesis of silver nanoparticles for antimicrobial applications: A green expertise. *Journal of Advanced Research*, 7(1), 17–28.
- Al Mashud, M. A., Moinuzzaman, M., Hossain, M. S., Ahmed, S., Ahsan, G., Reza, A., Anwar Ratul, R. B., Uddin, M. H., Momin, M. A., & Hena Mostofa Jamal, M. A. (2022). Green synthesis of silver nanoparticles using Cinnamomum tamala (Tejpata) leaf and their potential application to control multidrug resistant Pseudomonas aeruginosa isolated from hospital drainage water. *Heliyon*, 8(7), e09920.
- Anandalakshmi, K., Venugobal, J., & Ramasamy, V. (2016). Characterization of silver nanoparticles by green synthesis method using *Pedalium murex* leaf extract and their antibacterial activity. *Applied Nanoscience*, 6(3), 399–408.
- Aouf, D., Khane, Y., Fenniche, F., Albukhaty, S., Sulaiman, G. M., Khane, S., Henni, A., Zoukel, A., Dizge, N., Mohammed, H. A., & Abomughaid, M. M. (2024). Biogenic silver nanoparticles of *Moringa oleifera* leaf extract: Characterization and photocatalytic application. *Nanotechnology Reviews*, 13(1).
- Aragaw, T. A., Bogale, F. M., & Aragaw, B. A. (2021). Iron-based nanoparticles in wastewater treatment: A review on synthesis methods, applications, and removal mechanisms. *Journal of Saudi Chemical Society*, 25(8), 101280.
- Ashrafi-Saiedlou, S., Rasouli-Sadaghiani, M., Fattahi, M., & others. (2025). Biosynthesis and characterization of iron oxide nanoparticles fabricated using cell-free supernatant of *Pseudomonas fluorescens* for antibacterial, antifungal, antioxidant, and photocatalytic applications. *Scientific Reports*, 15, 1018.
- Bhattacharjee, R., Jha, S., & Roy, D. (2023). Synthesis, characterization and biomedical application of iron oxide nanoparticles. *Materials Chemistry and Physics*, 302, 127–134.
- Blaser, S. A., Scheringer, M., MacLeod, M., & Hungerbühler, K. (2008). Estimating the 'natural' environmental concentrations of silver and its compounds. *Science of The Total Environment*, 389(2–3), 351–358.
- Bordbar, A. K., Moghdami, S., & Ghorbani, M. (2014). Synthesis and characterization of magnetite nanoparticles via microwave assisted reaction and their application in dye removal from aqueous solution. *International Journal of Molecular Sciences*, 15(12), 22951–22961.
- Brahmachari, U. (2001). The Moringa tree: A miracle tree. *Journal of Medicinal Plants Research*, 5(1), 1–5.
- Chernousova, S., & Epple, M. (2013). Silver as antibacterial agent: Ion, nanoparticle, and metal. *Angewandte Chemie International Edition*, 52(6), 1636–1653.
- Chávez-Granados, Rodrigo, Martínez, Gabriela, García, Eduardo, Hernández, Carlos, & López, Silvia. (2024). Green synthesis of silver nanoparticles using natural hydrogel for antibacterial applications. *Gels*, 10(3), 398.
- Chen, Xiaoming, Li, Wei, Zhang, Yifan, & Zhou, Jing. (2017). Magnetite (Fe□O□) nanoparticles as bifunctional nanocomposite adsorbents for removal of both heavy metal ions and dyes. *Microwave and Nano Letters*, 12(1), 37–40.

- Coelho, N., Jacinto, J. P., Silva, R., Soares, J. C., Pereira, A. S., & Tavares, P. (2023). Green synthesis and antibacterial activity of silver nanoparticles obtained from *Moringa oleifera* seed cake. *Coatings*, 13(8), 1439.
- Dakal, T. C., Kumar, A., Majumdar, R. S., & Yadav, V. (2016). Mechanistic basis of antimicrobial actions of silver nanoparticles. *Frontiers in Microbiology*, 7, 1831.
- Dan-Kishiya, S., Okoro, G., & Olayemi, O. (2023). *Moringa oleifera*: A review of its nutritional and medicinal properties. *Journal of Medicinal Plants Studies*, 11(2), 45–50.
- El-Desouky, T. A., Salem, S. S., & El-Belely, E. F. (2021). Biosynthesis, characterization, and antibacterial activity of silver nanoparticles synthesized by *Aspergillus niger*. *Scientific Reports*, 11, 11172–11184.
- Esakkimuthu, T., Sivakumar, D., & Akila, S. (2014). Application of nanoparticles in wastewater treatment. *Pollution Research*, 33(3), 567–571.
- Gómez-Pastora, J., Bringas, E., & Ortiz, I. (2014). Recent progress and future challenges on the use of high performance magnetic nano-adsorbents in environmental applications. *Chemical Engineering Journal*, 256, 187–204.
- Fattah, B., Arif, H., & Hamzah, H. (2022). Antimicrobial and antibiofilm activity of biosynthesized silver nanoparticles against beta-lactamase-resistant Enterococcus faecalis. Applied Biochemistry and Biotechnology, 194(5), 2036-2046.
- Gowsalya, B., Ramesh, M., & Devi, A. (2024). Iron oxide nanoparticles: Green synthesis, characterization, and applications. *Environmental Nanotechnology, Monitoring & Management*, 22, 100774.
- Gurunathan, S., Kalishwaralal, K., Vaidyanathan, R., et al. (2014). Biosynthesis, purification and characterization of silver nanoparticles using *Escherichia coli*. *Colloids and Surfaces B: Biointerfaces*, 74(1), 328–335.
- Gutierrez, A. M., Dziubla, T. D., & Hilt, J. Z. (2017). Recent advances on iron oxide magnetic nanoparticles as sorbents of organic pollutants in water and wastewater treatment. *Reviews on Environmental Health*, 32(1–2), 111–117.
- Hamzah, H., Salah, R. F., & Maroof, M. N. (2018). Fusarium mangiferae as new cell factories for producing silver nanoparticles. Journal of Microbiology and Biotechnology. 28(10):1654-63. https://doi.org.10.4014/jmb.1806.06023
- Haris, Z., & Ahmad, I. (2024). Green synthesis of silver nanoparticles using *Moringa oleifera* and its efficacy against gram-negative bacteria targeting quorum sensing and biofilms. *Journal of Umm Al-Qura University for Applied Sciences*, 10, 156–167.
- Hua, Cheng, Wang, Lijun, Li, Yan, & Zhang, Hui. (2024). Rapid detection of pathogens using silver-graphene oxide composite and surface-enhanced Raman scattering. *Sensors*, 24(6), 1789.
- Jalal, A. F., & Fakhre, N. A. (2021). Preparation and Characterization of Green Fe3 O4 Nanoparticle Using the Aqueous Plant Extract of Gundelia tournefortii *L. ARO-The Scientific Journal of Koya University*, 9(2), 58–63.
- Jeol USA. (2022). Sample preparation techniques – Conductive coatings. Retrieved from Jeol USA resources.
- Jiang, X., Khan, S., Dykes, A., Stulz, E., & Zhang, X. (2025). Biogenic Synthesis of Silver Nanoparticles and Their Diverse Biomedical Applications. *Molecules*, 30(15), 3104.

● Karmakar, R., Sinha, S., Tripathi, H. S., Dey, S., Basu, S., & Meikap, A. K. (2023). Controlled growth of a highly energetic, less electron-dense tetrahedral Fe3+ phase on the surface of α-Fe2O3 nanoparticles toward enhanced optical, magnetic, and supercapacitive performance. *The Journal of Physical Chemistry C*, 127(26), 12502-12519.

● Khalil, M. M., Ismail, E. H., El-Baghdady, K. Z., & Mohamed, D. (2014). Green synthesis of silver nanoparticles using olive leaf extract and its antibacterial activity. *Arabian Journal of Chemistry*, 7(6), 1131–1139.

● Kiwumulo, H. F., Muwonge, H., Ibingira, C., Lubwama, M., Kirabira, J. B., & Ssekitoleko, R. T. (2022). Green synthesis and characterization of iron-oxide nanoparticles using *Moringa oleifera*: A potential protocol for use in low and middle income countries. *BioMed Central Research Notes*, 15(1), 1–8.

● Kortright, J. B., & Thompson, A. C. (2001). X-ray emission energies. In A. C. Thompson et al. (Eds.), *X-Ray Data Booklet* (2nd ed.). *Lawrence Berkeley National Laboratory*.

● Kumar, P., et al. (2024). Water purification and biological efficacy of green-synthesized Co/Zn-doped α-Fe□O□ nanoparticles. *Journal of Environmental Chemical Engineering*, 12(2), 1071–1082.

● Kyzas, G. Z., & Mitropoulos, A. C. (2021). Nanomaterials and nanotechnology in wastewater treatment. *Nanomaterials*, 11(6), 1539.

● Lesiak, Bartosz, Ciura, Katarzyna, & Kowalski, Piotr. (2019). FTIR investigation of Fe□O□ nanoparticles and nanocomposites with polysaccharides. *Frontiers in Chemistry*, 7, 642.

● Łach, Maciej, Nowak, Anna, & Sobczak, Marcin. (2023). Structural and functional FTIR analysis of proteins during nanoparticle synthesis. *Diagnostics*, 13(2), 123.

● Liao, S., Zhang, Y., Pan, X., Zhu, F., Jiang, C., Liu, Q., Cheng, Z., & Wang, X. (2019). Antibacterial activity and mechanism of silver nanoparticles against multidrug-resistant *Pseudomonas aeruginosa*. *International Journal of Nanomedicine*, 14, 1469–1487.

● Li, X., Xu, H., Chen, Z. S., & Chen, G. (2020). Biosynthesis of nanoparticles by microorganisms and their applications. *Journal of Nanomaterials*, 2020, 1–16.

● Li, X. F., & Mitch, W. A. (2018). Drinking water disinfection byproducts (DBPs) and human health effects: multidisciplinary challenges and opportunities. *Environmental science & technology*, 52(4), 1681-1689.

● Lopez-Garcia, M., Garcia, M., & Lopez, M. (2014). Synthesis and characterization of silver nanoparticles using plant extracts. *Journal of Nanoscience and Nanotechnology*, 14(6), 4383–4391.

● Madadi, M., & Mokhtarani, N. (2024). Selective recovery of silver from wastewater using Fe□O□@SiO□-SH magnetic composites. *Water, Air, & Soil Pollution*, 235(8), 487.

● Maestri, M., Polowczyk, I., & Zubair, M. (2017). Highly efficient removal of silver-containing nanoparticles in waters by aged iron oxide magnetic particles. *American Chemical Society Sustainable Chemistry & Engineering*, 5(7), 6000–6008.

● Mehwish, H. M., Rajoka, M. S. R., Xiong, Y., et al. (2021). Green synthesis of a silver nanoparticle using *Moringa oleifera* seed and its applications for antimicrobial and sun-light mediated photocatalytic water detoxification. *Journal of Environmental Science and Technology*, 15(3), 123–130.

- Mishra, P., Ray, S., Sinha, A., & Das, B. (2020). Green synthesis of silver nanoparticles using *Moringa oleifera* seed extract and its antibacterial activity. Materials Today: Proceedings, 29, 887–891.
- Mohammed, G. M., & Hawar, S. (2022). Green synthesis of silver nanoparticles from *Moringa oleifera* leaves extract and its antifungal and antitumor activities. *Heliyon*, 8(7), e09920.
- Mohammed, L., & Hamzah, H. (2024). Streptomyces pratensis-mediated fabrication of silver nanoparticles and its applications as Antimicrobial and Anticancer. BioNanoScience, 14(2), 1021-1032.
- Mohammadi, Parisa, Rezaei, Mohammad, & Farhadi, Kaveh. (2021). Green synthesis of iron-oxide nanoparticles using a fern extract for magnetically assisted removal of heavy metals. *Scientific Reports*, 11, 7893.
- Moodley, J. S., Krishna, S. B. N., Pillay, K., Sershen, F., & Govender, P. (2018). Green synthesis of silver nanoparticles from *Moringa oleifera leaf* extracts and its antimicrobial potential. Advances in Natural Sciences: *Nanoscience and Nanotechnology*, 9(1), 015011.
- Moustafa, M. T. (2017). Removal of pathogenic bacteria from wastewater using silver nanoparticles synthesized by two fungal species. *Water Science*, 31, 164–176.
- Poornima, S., Manikandan, S., Karthik, V., Balachandar, R., Subbaiya, R., Saravanan, M., Lan Chi, N. T., & Pugazhendhi, A. (2022). Emerging nanotechnology-based advanced techniques for wastewater treatment. *Chemosphere*, 303, 135050.
- Prachi, Gautam, P., Madathil, D., & Nair, A. N. B. (2013). Nanotechnology in wastewater treatment: A review. *International Journal of ChemTech Research*, 5(5), 2303–2308.
- Qu, X., Alvarez, P. J. J., & Li, Q. (2013). Applications of nanotechnology in water and wastewater treatment. *Water Research*, 47(12), 3931–3946.
- Qurbani, K., & Hamzah, H. (2021). Heavy metal tolerant comamonas species isolated from soil sample in Tanjaro region of Sulaymaniyah city-Iraq. Annals of the Romanian Society for Cell Biology, 25(5), 5068-5074.
- Rajeshkumar, S., & Bharath, L. V. (2017). Mechanism of plant-mediated synthesis of silver nanoparticles – A review on biomolecules involved, characterisation and antibacterial activity. Chemico-Biological Interactions, 273, 219–227.
- Ramirez, M., Ben Khalifa, E., Magnacca, G., Moreno, M. S., Parolo, M. E., & Carlos, L. (2025). Removal and recovery of Ag NPs from water by sustainable magnetic nanoflocculants. *Polymers*, 17(5), 650.
- Sharma, V., & Sharma, A. (2012). Nanotechnology: An emerging future trend in wastewater treatment with its innovative products and processes. *International Journal of Enhanced Research in Science, Technology & Engineering*, 1(2), November 2012.
- Sun, J., Chen, Y., Yu, H., Yan, L., Du, B., & Pei, Z. (2018). Removal of Cu^{2+} , Cd^{2+} , and Pb^{2+} from aqueous solutions by magnetic alginate microspheres based on Fe_3O_4 /MgAl-layered double hydroxide. *Journal of Colloid and Interface Science*, 532, 474–484.
- Thermo Fisher Scientific. (2019). Sputter coating for SEM: How this sample-preparation technique assists your imaging. *Advancing Materials* blog.
- Vance, M. E., Kuiken, T., Vejerano, E. P., McGinnis, S. P., Hochella, M. F., & Hull, D. R. (2015). Nanotechnology in the real world: Redeveloping the nanomaterial consumer products inventory. *Beilstein Journal of Nanotechnology*, 6(1), 1769–1780.

- Varthini, T., & Carmel Vigila Bai, G. M. (2018). Biogenic synthesis of silver nanoparticles using *Moringa oleifera* seeds and its structural investigation. *International Journal of Trend in Research and Development*, 5, 45–48.
- Vernieres, J., Proust, J., & Plain, J. (2021). Laser-induced deposition of plasmonic Ag and Pt nanoparticles: SEM/EDS identification of Ag with a 2.98 keV Lα line. *Materials, 14*(1), 10.
- Yass, R., Mohammed, S., Jalal, T., & Hamzah, H. (2024). Evaluation of physiochemical, heavy metals, and bacteriological parameters of celery and its irrigation water within Sulaymaniyah city of Iraq. Environmental Monitoring and Assessment, 196(5), 483.
- Yew, Y. P., Shameli, K., Miyake, M., Kuwano, N., & Khairudin, N. B. B. (2023). Green synthesis of magnetite nanoparticles using *Labisia pumila* leaves extract and its biomedical applications. *Arabian Journal of Chemistry*, 16(1), 104–118.